Physicochem. Probl. Miner. Process., 60(4), 2024, 191375

http://www.journalssystem.com/ppmp

Physicochemical Problems of Mineral Processing

ISSN 1643-1049

Numerical investigation of the impact of various parameters on blowing accuracy in the XRT intelligent ore sorting machine blowing process

Jiayu Fan [1,2], Yuhuan Rao [1,2,3], Sidong Liu [1,2], Xinyang Yu [1,2]

[1] School of Resources and Environmental Engineering, Jiangxi University of Science and Technology, Ganzhou 341000, Jiangxi, China

[2] Jiangxi Province Key Laboratory of Mining Engineering, Ganzhou 341000, Jiangxi, China

[3] Slon Magnetic Separator Co. Ltd., Ganzhou 341000, Jiangxi, China

Corresponding author: 172004588@qq.com (X. Yu)

Abstract: XRT separation equipment is attracting much attention as the mining industry increasingly uses pre-sorting technology. Its sorting accuracy is affected by differences in ore shape and particle size during operation. This paper, in which numerical simulations are conducted to investigate the resistance of ores under various situations, including varying blowing distances, cross-sections, and practical sizes, Additionally, this paper conducts validation tests. The test results indicate that within the 0.1-0.25 m section from the nozzle exit, there is a rapid decrease in velocity, accompanied by a significant change in ore resistance. Beyond the 0.25 m mark, the velocity reduction slows down, while the ore resistance becomes smaller. There exists a notable disparity in the resistance of ores with varying cross-sectional geometries. The size of the jet velocity surface caused by blowing distance significantly influences the resistance of ore with varying particle sizes. Furthermore, the resistance of the ore remains constant subsequent to the impact surface of the ore surpassing the surface of the jet velocity. Consequently, appropriately modifying the blowing distance, inlet pressure, and jet speed in accordance with the cross-sectional area and particle size of the majority of the ores stream can enhance the precision of the sorting process.

Keywords: intelligent sorting machine, pre-selection for waste, ore blasting, ore stresses, numerical simulation

1. Introduction

The depletion of mineral resources is becoming increasingly serious due to the ongoing extraction of domestic ores. To address this issue, a mining X-ray intelligent sorting machine is employed to separate waste from the ore prior to its entry into the mill, so achieving the objective of pre-enrichment (Ilankoon et al., 2018; Luo et al., 2022). Several studies have been conducted both domestically and internationally on the topic of pre-sorting and eliminating waste ore equipment. However, it is worth noting that the majority of studies on jet flow fields of such equipment have been conducted in other domains, with very limited investigations conducted specifically in the realm of ores. Regarding the applied research field concerning XRT apparatus, Zhang et al. (2021) investigated the method for distinguishing the properties of sulfide and non-sulfide minerals in order to ascertain their composition and evaluated the sorting capability of dual-energy XRT pre-sorting equipment between sulfide minerals and waste rock. Yeyu et al. (2021) classified aluminum and magnesium in waste metals via multi-energy X-ray transmission and forecasted the optimal recognition rate for aluminum and magnesium using machine learning. In the field of trash recycling, Duvillier et al. (2018) utilized dual-energy X-ray the transmission to identify and classify materials, meanwhile put forward achieved this by integrating the outcomes obtained from both virtual and actual measurements. In the domain of optimization for intelligent sorting equipment. Bauer et al. (2022) evaluated the feasibility of DEM-CFD modeling for the

DOI:

optimization design of intelligent sorting equipment, with the equipment optimized by changing the two parameters of conveyor speed and nozzle response time. Pieper et al. (2018) constructed a computational model to simulate intelligent sorting equipment. This model utilized a coupled approach combining the discrete element method and computational fluid dynamics. The research examined the sorting efficacy of employing a face array camera and particle tracking combination for specific sorting scenarios. The results indicated a high degree of adaptability for this combined approach to sorting ores. Küppers et al. (2021) made a comparison between the throughput, product purity, recovery, and misselection rate of SBS equipment at various throughput rates and graphical representations of the obtained results, which were subsequently utilized to enhance the performance of the equipment. In the domain of nozzle investigation pertaining to ore sorting machinery. Zhu et al. (2016) used numerical simulation to look into the flow fields of conical and conical-straight nozzles. They looked at a number of conditions, such as different nozzle structures, outlet radii, and constriction angles. To make sure the simulations were accurate, they then did experiments to measure how far the ore actually blew from the different types of nozzles. Within the domain of food categorization. Chen et al. (2020) devised a vision-based recognition approach for the purpose of segregating tea leaves that are intermingled with aged and fragmented ones. In other fields, Chen et al. (2023) employed computational fluid dynamics to conduct an analysis and optimization of flushing nozzles within the drilling industry. Zhong et al. (2023) examined the expansion angle, jet width, and jet penetration depth of gas jets within gas-solid fluidized beds featuring various nozzle inclination angles and, meanwhile, developed a mathematical model of the inclined jet. Cristofaro et al. (2020) examined, in order to enhance the longevity of diesel engines, the correlation between the geometry of a diesel injector nozzle and its geometry subsequent to corrosion.

There is a limited body of research available on the application of nozzles in sorting equipment, particularly in the context of ore separation, both domestically and internationally. Intelligent sorting equipment actuators in the design and production process are often based on practical experience, with debugging equipment inlet pressure, nozzle exit diameter, and so on driven to reach the functioning conditions. During the sorting process, several factors, such as particle size, shape, ore type, and ore grade, can lead to misblowing. Therefore, numerical simulation of the blowing distance, common cross-sectional shapes, and the laws governing various ore particle sizes in the separation process is required to guide the design of the equipment's structure when the jet flow field remains constant. Hence, it is of practical significance to employ ANSYS-Fluent software for the numerical simulation of the ore separation process in the intelligent ore sorter, as well as to validate the rationality of the numerical simulation through experimental investigations. This approach assists in the design of actuators, sorting bins, and other components of the intelligent ore sorter.

2. Nozzle, ore modeling and force analysis of ore

The ore sorting process involves several steps. Initially, the ore is fed into the feed hopper. From there, it passes through a vibrating feeder, which helps to loosen the flow of the ore. Subsequently, the ore is transported forward using a conveyor belt transmission, with its speed determined by the conveyor belt. Upon traversing the irradiation zone, the ore undergoes exposure to X-rays and subsequently passes identification via a detector. Following it, image processing methods are used. Based on the results of these grayscale image processes, a nozzle begins to selectively blow air, separating the valuable ore from the waste rock. The utilization of a conveyer belt in an ore sorting machine involves a sorting process that may be classified as parabolic motion. The conveyer belt's speed determines the ore's initial velocity, known as V_0. As depicted in Fig. 1, the ore is propelled in either a flat throwing curve track or an upward sloping arc track due to the combined effects of blowing force and conveyer belt speed. The magnitude of the local gravitational acceleration is about 9.8 m/s^2, and the test equipment sets the initial speed of the conveyor belt V_0 at 3 m/s. The nozzle determines the values of blowing force F and velocity V_F.

The efficiency of the XRT intelligent ore sorting machine sorting process is primarily influenced by two factors: the precision of ore identification and the accuracy of the executing agency's blowing on the ore. The executive agency comprises many components, including an air compressor, air drying machine, air storage tank, pipeline, solenoid valve, valve group, and blowing plate, shown in Fig. 2. The

DOI: 10.37190/ppmp/191375

air compressor is responsible for generating compressed gas, which is then passed through an air drying machine and a compressed air filter. The high-pressure gas is subsequently conveyed through a series of pipes to reach a small storage tank the located beneath valve group. When the solenoid valve is activated, the nozzle sprays a jet of compressed air, which has a significant influence on the accuracy of ore sorting.

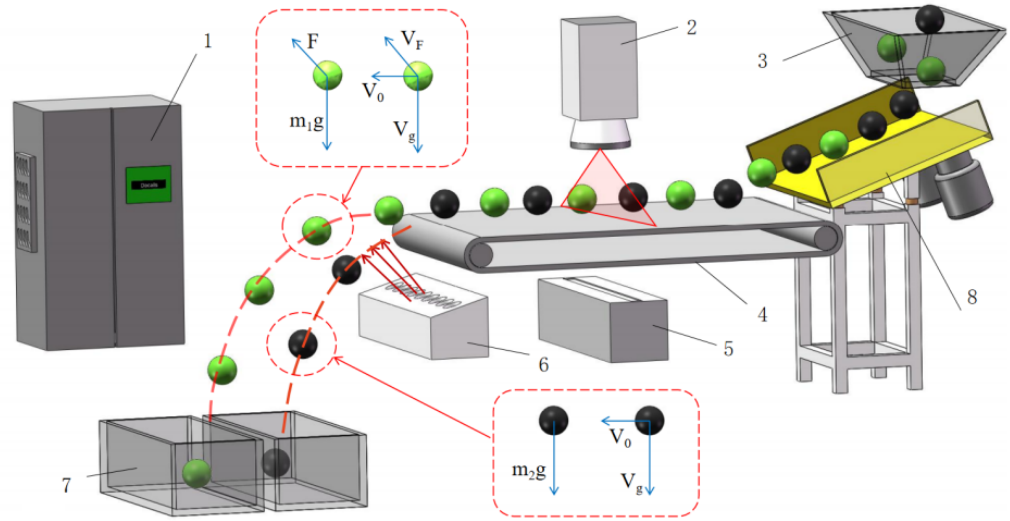

1-control cabinet; 2-radiation source; 3-feed hopper; 4-conveyor belt; 5-detector; 6-blowing plate; 7-ore sorting bin; 8-vibrating feeder

Fig. 1. Schematic diagram of force separation of useful ore and waste rock

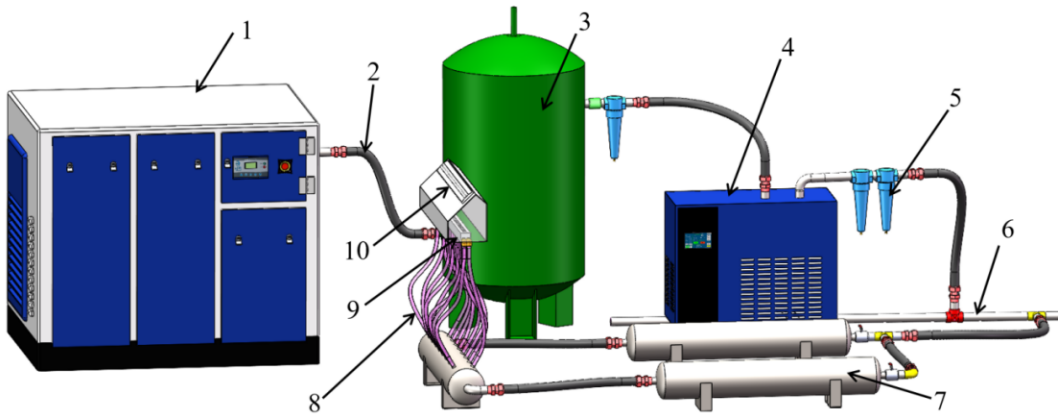

1-air compressor; 2-rubber tube; 3-large gas storage tank; 4-air drying machine; 5-compressed air filter; 6-long steel pipe; 7-small gas storage tank; 8-PU gas tube; 9-solenoid valve group; 10-blowing plate

Fig. 2. Schematic diagram of XRT intelligent ore sorter actuator

2.1. Nozzle modeling and meshing

In this paper, we have tested a production machine for sorting grain sizes from 8 to 80 mm. The nozzle structure is depicted in Fig. 3(a). For optimal computational efficiency and the small step has little effect on the simulation; we present the change structure shown in Fig. 3(b).

For the purpose of improving the computational efficiency of the simulation, the analysis of the flow field is exclusively conducted on the central, two-dimensional cross-section of the nozzle. The flow field range outside the nozzle is set to be 100×20 times the nozzle exit R2. The encryption of the grid at the nozzle exit is necessitated by the presence of high-speed turbulence and significant pressure variations. This encryption results in a total of 48,649 grid cells, as shown in Fig. 4. Based on the nozzle operating

DOI: 10.37190/ppmp/191375

time, working fluid properties, and other relevant conditions, this paper utilizes a transient density-based implicit solver. The boundary conditions are specified as pressure inlet and pressure outlet, while the near-wall region is handled using the scalable wall function.

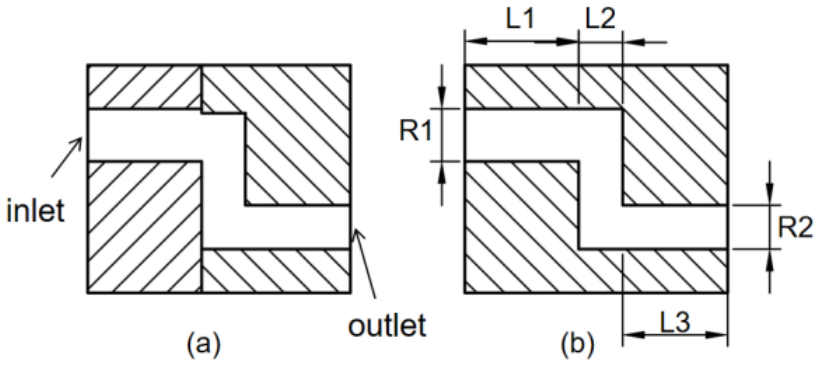

Fig. 3. Schematic diagram of nozzle structure

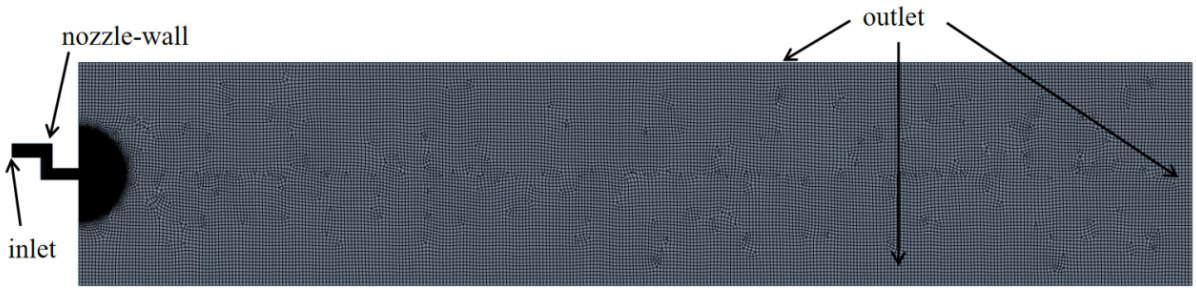

Fig. 4. Schematic diagram of nozzle and external flow field meshing

2.2. Turbulence model and control equations

The air stream emitted from the ore separation nozzle serves as a high-velocity jet employed for the purpose of generating an impact. The phenomenon under consideration involves the injection of a high-velocity jet into an environment characterized by a significantly lower flow velocity. In this scenario, the jet can be conceptualized as a free submerged jet. The flow field of a jet demonstrates a substantial amount of complexity. In addition to the fundamental equations of continuity and momentum, the energy equation must also be taken into account. This is due to the reality that at high flow velocities, there is a conversion of internal energy into mechanical or kinetic energy. The continuity equation is shown in Eq. (1).

$$\frac{\partial \rho}{\partial t} + \nabla(\rho \boldsymbol{u}) = 0 \tag{1}$$

The momentum equation is shown in Eq. (2) and Eq. (3).

$$\frac{\partial \rho}{\partial t} + \nabla(\rho u \boldsymbol{u}) = \nabla(\mu \text{grad } u) - \frac{\partial \rho}{\partial x} + S_u \tag{2}$$

$$\frac{\partial \rho}{\partial t} + \nabla(\rho v \boldsymbol{u}) = \nabla(\mu \text{grad } v) - \frac{\partial \rho}{\partial y} + S_v \tag{3}$$

The energy equation is shown in Eq. (4).

$$\frac{\partial(\rho T\})}{\partial t} + \nabla(\rho T \boldsymbol{u}) = \nabla\left(\frac{k}{c_p} \text{grad } T\right) + S_T \tag{4}$$

In this context, represents the divergence, corresponds to the density, t signifies the time, denotes the velocity vector, and are the velocity vector's components in the and directions respectively. The term "grad" refers to the gradient, while and are the generalized source terms of the momentum equation. stands for the constant-pressure specific heat capacity, represents the temperature, denotes the heat transfer coefficient of the fluid, and signifies the viscous dissipation rate (Zucker, Biblarz, 2019; Kannan, Foias, 1988).

The Realizable k-epsilon model is employed to represent turbulence, in which the buoyancy part is not included (Ahmed, Ovinis, 2019; Kannan et al, 2017). The transport equation for this model is shown in Eq. (5) and Eq. (6).

$$\frac{\partial(\rho k\})}{\partial t}+\frac{\partial}{\partial x_j}(\rho k u_j)=\frac{\partial}{\partial x_j}\left[\left(\mu+\frac{\mu_t}{\sigma_k}\right)\frac{\partial k}{\partial x_j}\right]+G_k\text{-}\rho\varepsilon \tag{5}$$

$$\frac{\partial(\rho\varepsilon\})}{\partial t}+\frac{\partial}{\partial x_j}(\rho\varepsilon u_j)=\frac{\partial}{\partial x_j}\left[\left(\mu+\frac{\mu_t}{\sigma_\varepsilon}\right)\frac{\partial\varepsilon}{\partial x_j}\right]+\rho C_1 S\varepsilon\text{-}\rho C_2\frac{\varepsilon^2}{k+\sqrt{\nu\varepsilon}} \tag{6}$$

In this context, $C_1=max\left[0.43,\frac{\eta}{\eta+5}\right],\eta=S\frac{k}{\varepsilon},S=\sqrt{2S_{ij}S_{ij}},C_2=1.9,\mu_t=\rho C_\mu\frac{k^2}{\varepsilon},A_0=4.04,A_s=\sqrt{6}\cos\varphi,\sigma_k=1.0,\sigma_\varepsilon=1.2$, k denotes the turbulent kinetic energy , and ε signifies the turbulent dissipation rate, see more details in (Fluent, 2023) .

2.3. Modeling of test ores

The shape and quality of the ore cannot be standardized due to its complexity. This research involved the analysis of a specific batch of tungsten ore, which was carefully selected based on particle size and cross-section shape. Representative samples were chosen from this batch, and the cross-section shapes were categorized into five groups: oblate quadrilateral, quadrilateral, polygonal, triangular, and semicircular arc. Fig. 5 depicts a representative image of an ore sample.

The simulation time can be efficiently reduced by representing the complicated ore with appropriate simplified geometry, due to the intricate nature of the ore. The simplified results are shown in Fig. 6.

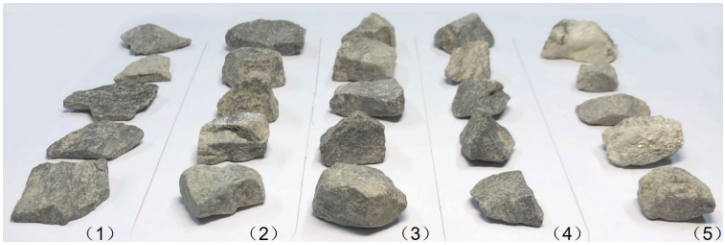

Fig. 5. ore grouping

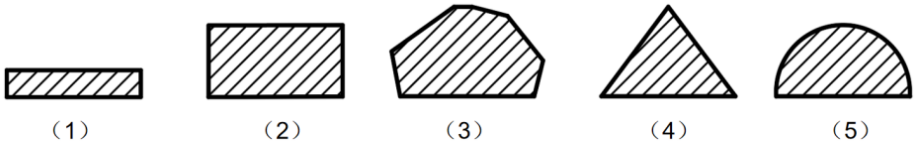

Fig. 6. Schematic diagram of simplified modeling of ore cross section

3. Simulation results and analysis

3.1. Jet flow field simulation results

Following the previously mentioned steps, which include parameter configuration, the resulting figures, namely Fig. 7 and Fig. 8, depict the outlet R2 with a diameter of 5 mm, as well as the velocity cloud image of the jet flow field and the axial velocity distribution of the external flow field.

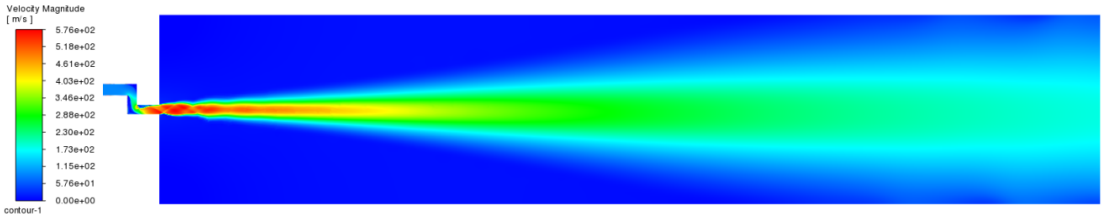

Fig. 7. Velocity distribution cloud image of jet flow field

At an inlet pressure of 0.8 MPa, the maximum velocity for the entire flow field is 575.846 m/s, while for the external flow field, it is 568.376 m/s. The entirety of the jet can be classified as a supersonic,

underexpanded free jet. At the exit, the jet undergoes radial expansion, resulting in the reflection of an expansion wave as a compression wave at the jet's boundary. These two waves combine to form a surge wave, which is inclined toward the airflow. Despite the presence of the surge wave, the airflow behind it remains supersonic. As the flow passes through the surge wave, it undergoes further compression due to the reflected surge wave and separates from the flow behind the Mach disk through a slip line. Along the axis of the jet, the pressure gradually decreases until it reaches the ambient pressure (Hatanaka, Saito, 2012; Lai, 2023). Therefore, discernible variations in velocity occur within a range of 0-0.1 meters. Due to the presence of substantial internal deflection within the nozzle construction, the outlet section's length is insufficient, leading to a minor deflection of the overall external flow field towards the underregion (George, 2021). For the purpose of streamlining the modeling procedure, we make the assumption that the relative location of the ore remains constant as it moves away from the belt and that the central axis of the jet is precisely aligned with the center of the ore. After 0.25 m, the velocity decrease trend of the jet becomes less pronounced, whereas the degree of velocity diffusion progressively increases until the jet velocity attains zero.

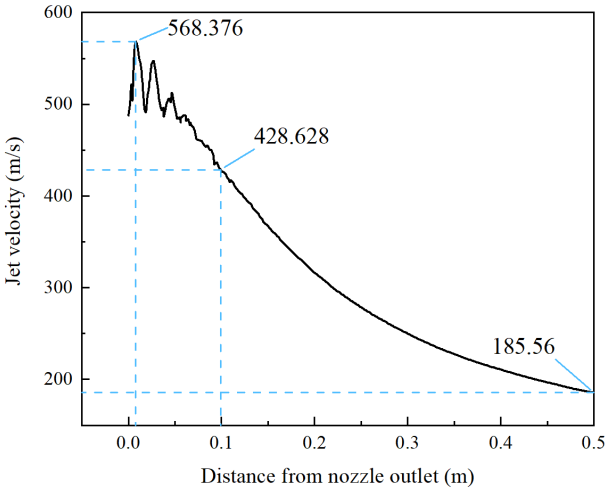

Fig. 8. Axial velocity distribution profile of the flow field outside the nozzle

3.2. Simulation of ore blowing at different distances

The XRT intelligent sorting machine has the capability to adjust the position of the blowing plate based on specific requirements. These locations include lower and upper placements, shown in Fig. 9.

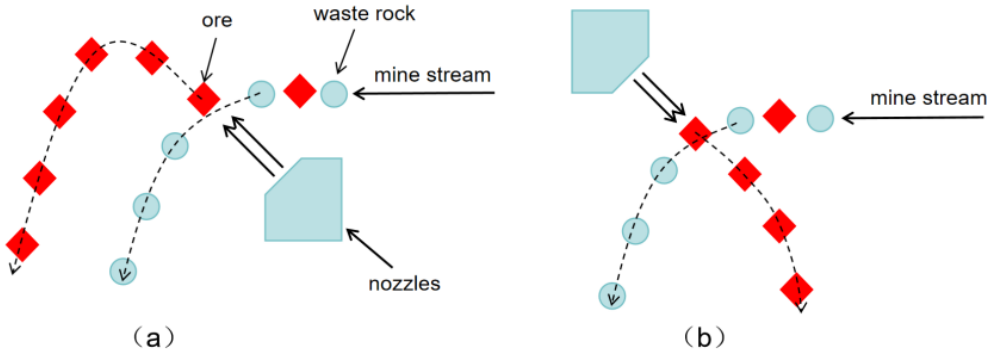

Fig. 9. Schematic of the difference between lower and upper blowing plate assemblies

The installation position of the nozzle assembly affects the distance at which the jet impacts the ore, resulting in significant variations. Moreover, there is a substantial difference in jet velocity within a 0.1 m range, which leads to instability in the ore blowing process. After reaching a distance of 0.5 m, the velocity decreases to 185.56 m/s. This reduction in velocity may result in insufficient blowing force due to excessive diffusion. Consequently, the flow field analysis will focus on the region after 0.1 m and

before 0.5 m. A simulation was carried out to investigate the resistance experienced by a 15×8 mm rectangle-shaped ore cross-section when subjected to a jet blowing at various distances from the nozzle outlet position. The distances considered were 0.1, 0.15, 0.2, 0.25, 0.3, 0.35, 0.4, and 0.45 m. A simulation is conducted to model the effect of a jet blowing on the ore under a fixed working condition. The resistance force exerted on the ore is monitored in order to establish a correlation between the blowing distance and velocity and the resulting impact force on the cross-section of this particular type of ore. These findings are visually represented in Fig. 10.

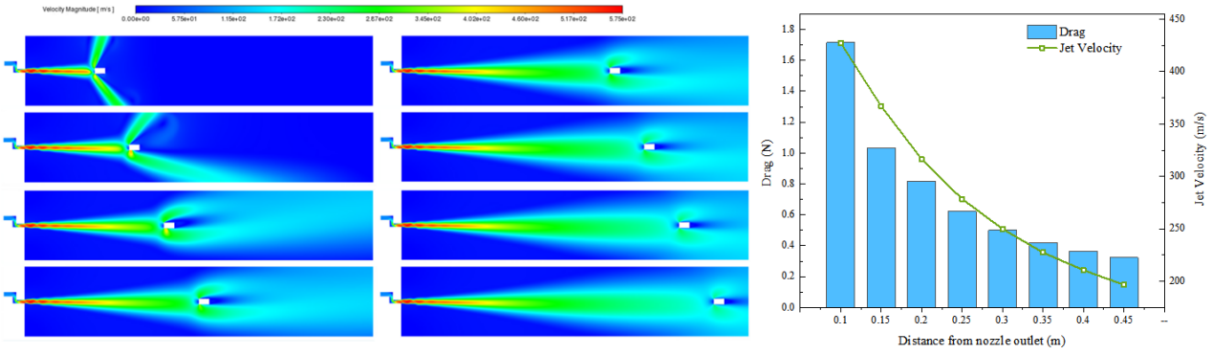

Fig. 10. Impact of jet on ore at different locations in the external flow field

The results indicate that during the 0.1-0.25 m division by an increasingly quick drop in velocity, the resistance experiences a substantial decrease from 1.715 N to 0.621 N. In contrast to the 0.3-0.5 m division, where the velocity decrease is more gradual, the resistance exhibits a slower decline from 0.499 N to 0.323 N. In the context of ore sorting, it is important to ensure a higher degree of stability in the trajectory of the ore. The blowing distance of a jet impact force on a given piece of ore alters depending on the conditions. Therefore, it is necessary to adjust the blowing distance for different ores based on factors such as particle size and quality.

3.3. Simulation of resistance to different cross-sections of ore

Based on the ore model depicted in Fig. 6, several cross-section ores characterized by a grain size of 15 mm are simulated at distinct positions within the flow field. The outcomes of these simulations are shown in Fig. 11.

The left-hand cloud image seen in Fig. 11 displays the four ore cross-sections, following the sequence of Fig. 6, with the exception of the quadrilateral cross-section. The simulation results of the four different cross-section ores are consistent with the numerical simulation trend described above. The flat quadrilateral (flaky ore) exhibits a small force surface, resulting in a small force range with a maximum of 0.817 N and a minimum of 0.141 N. The semi-circular arc cross-section ore, characterized by a force surface that is a circular curved surface, also experiences a small force range with a maximum of 1.135 N and a minimum of 0.239 N. The quadrilateral cross-section ore demonstrates the most significant resistance trend, with the resistance of the quadrilateral, polygonal, and triangular cross-section ores being similar in magnitude after a distance of 0.15 m.

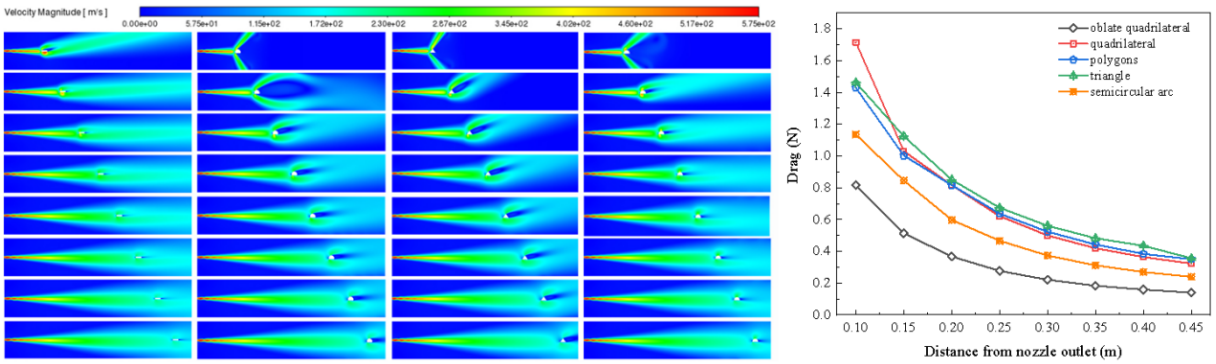

Fig. 11. Jet impingement on ores of different cross-sections

DOI: 10.37190/ppmp/191375

The results show that the sorting of flake and semicircular arc ores is more stringent with respect to the distance requirement than the other three cross-sections of ores. For these two types of ores, decreasing the blowing distance can increase the blowing strength, which is conducive to improving the blowing accuracy. The stability of the sorting process for the other three types of ores is higher in the middle section, where the velocity is stable.

3.4. Simulation of resistance to different particle size of ore

The ore sorting process is affected by several factors, including the size of the ore particles as well as the distance and cross-sectional form. The test equipment used in this study has a theoretical sorting ore particle size interval ranging from 8 mm to 80 mm. To ensure consistency, the particle size of the ores with the aforementioned cross-section shape was incrementally raised by 7 mm, starting from 8 mm and progressing up to 80 mm. The simulation outcomes at distances of 0.1 m and 0.3 m from the exit location are depicted in Fig. 12 and Fig. 13, respectively.

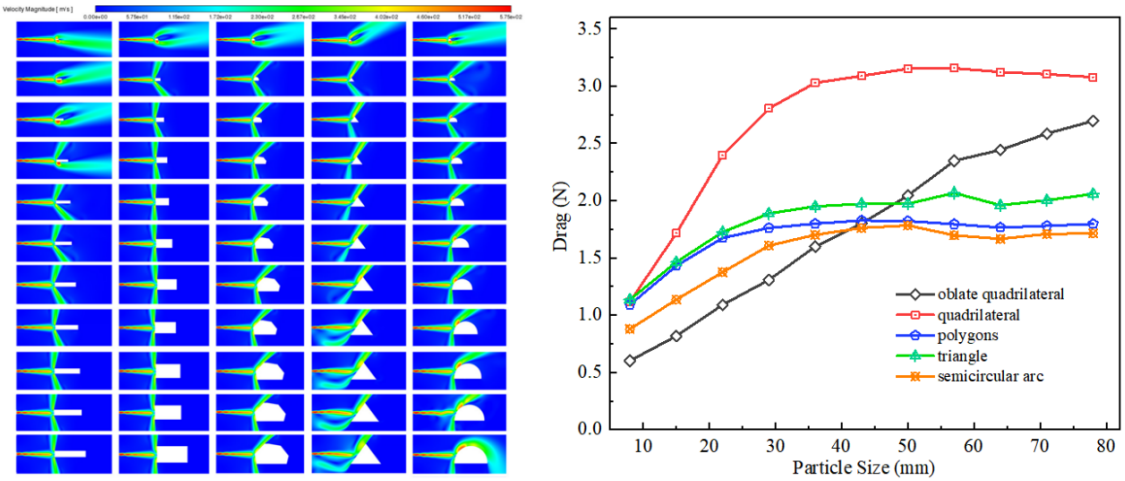

Fig. 12 Jet impact on ore of different cross section and grain size at 0.1 m from nozzle outlet

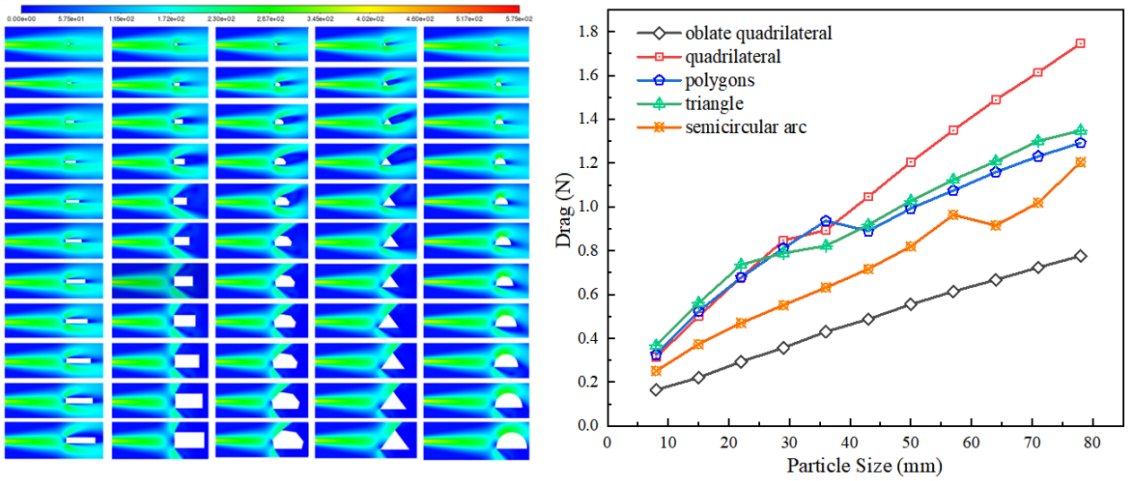

Fig. 13. Jet impact on ore of different cross section and grain size at 0.3 m from nozzle outlet

The sorting accuracy of a jet-based sorting process is negatively affected by the particle size of the ore. However, narrowing down the selected ore fraction leads to excessive energy consumption during pre-classification. Therefore, it is common practice to limit the range of ore fractions in the ore stream entering the sorting machine to a wider range. Therefore, enhancing the correlation between the distance of blowing and the particle size of the entering ore is a crucial element in enhancing the accuracy of the sorting process. When the diameter of the jet cross-section increases, if the impact surface of the ore is smaller than the jet cross-section, the jet will exhibit a phenomenon where it flows around

DOI: 10.37190/ppmp/191375

the ore. The observation depicted in Fig. 12 reveals that the jet flow ceases to experience flow around an oblate quadrilateral ore after the grain size of the ore reaches 36 mm, when the distance from the nozzle exit is 0.1 m. The remaining four cross-sections of the ore experience a larger impact surface from the jet compared to the oblate quadrilateral ore. After reaching a distance of 15 mm from the flow, no further occurrences are observed. Subsequently, as the impact surface of the jet increases, the resistance of the ore is found to be proportional to the increase in particle size. When the grain size of the ore reaches 36 mm, the jet velocity escape surface exceeds the cross-section size of the impact surface area of the ore. Consequently, the impact of the jet on the ore becomes very stable, and the resistance of the ore remains largely unaltered in terms of size. As illustrated in Fig. 13, when 0.3 m from the nozzle outlet, the resistance of the ore increases with the particle size, and there is no stable resistance section because the jet velocity escape surface is greater than the impact surface of the ore.

3.5. Effect of different inlet pressures on blowing force

Through the above simulation, it can be seen that the particle size has a great influence on the resistance of the ore particles, which is reflected in the fact that the resistance of the fine size ore is much smaller than that of the large size ore. By changing the pressure conditions of the inlet, improving the jet strength can effectively improve the resistance of fine size ore. When the fine size ore accounts for the majority of the ore flow, this method can make the fine size ore resistance close to the large size ore, which in turn makes the sorting accuracy improve.

In different inlet pressure conditions, the blowing distance is 0.1 m. The size of the resistance of different cross-sections of ore particles with a particle size of 15 mm is shown in Fig. 14.

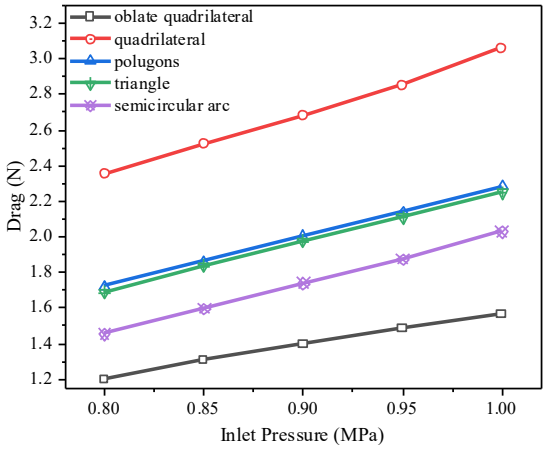

Fig. 14. Ore of different cross sections resisted at different inlet pressures

The combination of Fig. 12 and 14 shows that there is a large gap between the force on 15 mm ore particles and 35 mm ore particles when the inlet pressure is 0.8 MPa. The resistance at an inlet pressure of 1 MPa and an ore size of 15 mm is close to that at an inlet pressure of 0.8 MPa and an ore size of 35 mm. Therefore, when there are more small particles ore in the ore stream and there is a certain proportion of large particles ore, increasing the inlet pressure to 1 MPa can increase the distance of small ore particles to be blown away, thus reducing the leakage phenomenon due to insufficient blowing force.

4. Verification tests

The validation test establishes a simple test platform system, which includes components such as fixed nozzles and solenoid valve groups, and validates the simulation results through two types of tests: measuring the distance at which the ore is blown away and testing the ore leakage rate by the real machine on a small batch of ores.

4.1. Ore blowing distance test

The experiment on ore blowing distance is categorized into three types. In the first type, a rectangular cross-section ore is chosen for testing at various distances, and the outcomes are depicted in Fig. 15 (a).

In the second type, five ores with different cross-sections but similar particle sizes are selected for testing at different distances, and the results are presented in Fig. 15 (b). Lastly, the third type involves the selection of eleven ores with varying particle sizes for testing at a consistent distance, and the results are displayed in Fig. 16.

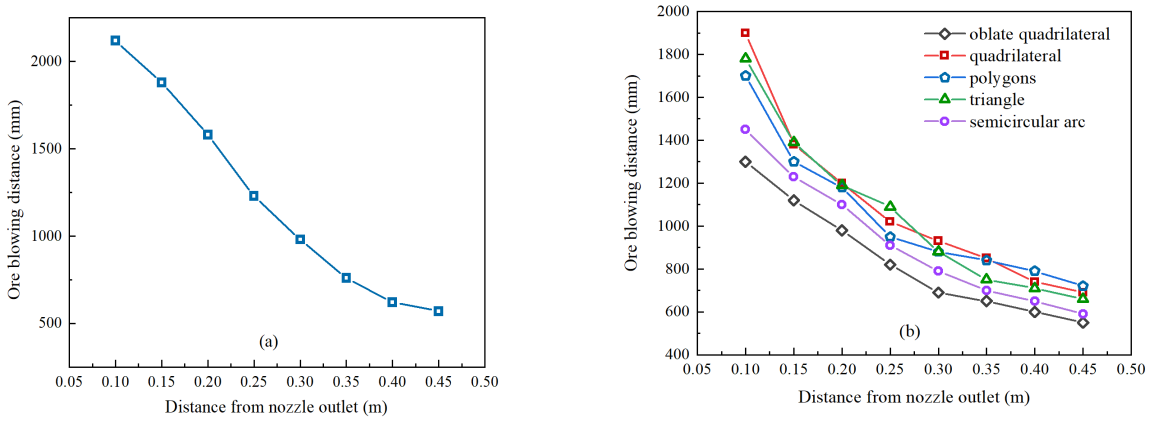

Fig. 15. Results of different cross-section ores subjected to blowing at different distances

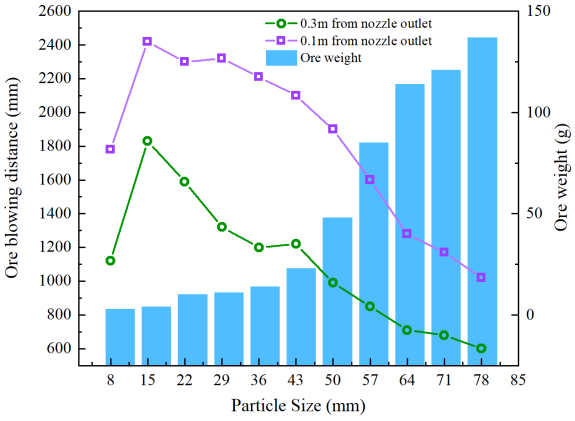

Fig. 16. Results of different grain size ores subjected to blowing at different distances

The test findings indicate an inverse relationship between the distance at which ore is blown away and the blowing distance. This finding aligns with the expected resistance situation resulting from changes in the cross-sectional area. In the same type of ore, the relationship between mass and particle size is directly proportional, whereas the relationship between mass and ore blowing distance is inversely proportional. The variation in ore blowing distance is more violent at 0.1 m than at 0.3 m as particle size and mass increase, but the ore blowing distance between the two places is roughly twice at the same particle size. Due to the pre-designed structure dictating the distance between the nozzle outflow jet's contact with the ore, disruptions to the sorting process are easily introduced during periods of rapid velocity changes; the interference is greatest at the fine grain level of the ore. In the process of sorting ores of significant size, it is possible to narrow down the blowing distance to around 0.2 m by analyzing the approximate particle size of the ore. During this stage, it is found that adjusting the blowing plate in an upper location is more suitable. The sorting accuracy of ores with a medium particle size is not significantly influenced by the blowing distance. For small-size ores, the blowing distance should be chosen in a region where the velocity changes slowly, and it should be more exact. This effectively avoids errors induced by too much or too little blowing force.

4.2. Small batch ore leakage rate test

Test using ore for a mine 8-80 mm tungsten ore, according to 8-15 mm, 15-25 mm and so on 7 grades of granularity classified, the mass of each grade of ore in the 20 kg to 30 kg, to get in the same belt speed

DOI: 10.37190/ppmp/191375

conditions, the blowing distance is about 0.2 m, the leakage rate of the 7 kinds of granularity tungsten ore, as shown in Fig. 17.

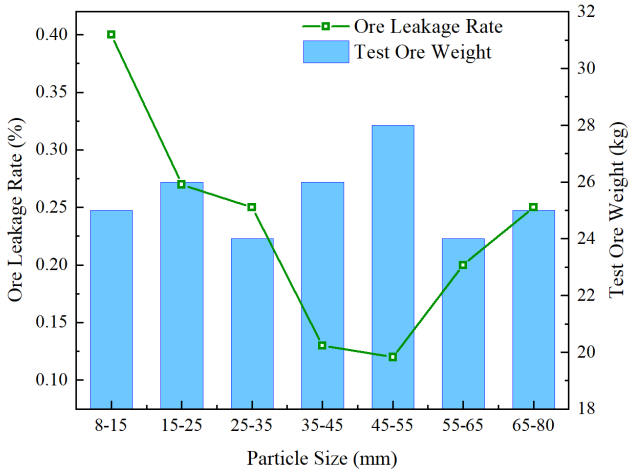

Fig. 17. The size of the leakage rate of different particle size ores

The ore leakage rate refers to the ratio of the weight of the ore falling in the other sorting bin to the total weight of the test ore entering the equipment when the equipment is set to full blow mode. The test results show that the ore leakage rate is largest when sorting fine grade ore and reaches a minimum in the intermediate grade, and this blowing distance has a low probability of misclassification for the intermediate grade ore. This trend is consistent with the previous result that when blowing different sizes of ore, the force is small for fine size ore and great for large size ore, and that the mass of the ore also has an effect on the blowing distance when it is oversized.

All the above grades of ore particles were re-blend and then tested by blowing, obtaining a leakage rate of 0.87%. The fine particle size ore of 8–15 mm in grain size was further tested after removing the ore particles from the batch, and the leakage rate was obtained as 0.47%. It is shown that reducing the particle size distribution of the ore stream can improve equipment misselection.

In the same jet condition, the resistance of fine size ore particles is smaller than that of large size ore particles, which leads to misselection. The working pressure of the air compressor is set to 1MPa, and the ore particles of 8-15 mm and 15-25 mm are blown, and the leakage rate is 0.322% and 0.218%, respectively, which is a big improvement compared with the previous one.

5. Conclusions

To study the outside flow field of the ore blowing process, numerical simulations were run with different parameters, such as different blowing distances, different cross-sectional blowing ore forces, and different particle size blowing forces. Experimental testing followed to confirm the simulation results. Simulation and test results show that in the mechanical structure of the sorting bin, the nozzle with the design, through the control of the ore blowing distance, so as to achieve in the original equipment without changing the structure of the basis, effectively improve the sorting accuracy, the intelligent sorting machine sorting ore recovery rate has a certain role in improving.

(1) For different blowing distances on the same cross-section, particle size ore sorting accuracy has a large impact on the distance change of more than 0.25 m after the ore is subjected to lower resistance, for the impact of large ore may not be enough, so the jet stabilizes the front portion of the big density or large particle size ore blowing effect, which is much better than the back end.

(2) There's a relationship between the resistance of the ore and the shape of the jet impact surface at the same blowing distance and particle size. When the impact surface is linear as opposed to curved, the impact force that the ore experiences is greater. The magnitude of the impact force exerted on the ore is maximized when the jet achieves a vertical impact, whereas it is reduced when the jet strikes the ore at an oblique angle. By irradiating the ore stream with X-rays and getting a grayscale picture of the ore, the amount of a certain cross-section of the ore in the stream can be analyzed and

measured. Based on this analysis, adjustments can be made to the air inlet pressure or blowing distance in order to enhance or reduce the blowing force, thereby improving the accuracy of the sorting process.

(3) When the jet impact surface of the ore does not exceed the jet velocity escape surface, the magnitude of the ore resistance is directly proportional to the size of the jet impact surface, provided the same injection distance and cross-section conditions. The resistance of ore is affected by changes in particle size, leading to a significant difference in resistance in the same blowing position, typically ranging from three to four times. Hence, optimizing the blowing distance for varying particle sizes within the ore stream can greatly enhance sorting accuracy.

(4) Small size ore and large size ore due to the different size of the impact surface lead to different drag forces, which in turn lead to misselection. By identifying the proportion of fine size ores in the ore stream and adjusting the inlet pressure, the misselection of fine size ores due to insufficient impact force can be improved.

The limitation of this work is that only 2D simulation computations were performed, which did not accurately depict the ore's moving trajectory. At the same time, due to the variety of ore shapes in the ore flow, the shape of the ore used in the simulation is limited, resulting in some mistakes.

Acknowledgments

The authors would like to acknowledge the National Nature Science Foundation of China (No. 52264023) and "Double height project" of Jiangxi province [2022]223.

References

ILABKOO I, TANG Y, GHORBANI Y, et al., 2018. *The current state and future directions of percolation leaching in the Chinese mining industry: Challenges and opportunities. Minerals Engineering*. 125:206-222.

LUO X, HE K, ZHANG Y, et al., 2022. *A review of intelligent ore sorting technology and equipment development. International Journal of Minerals, Metallurgy and Materials*. 29(9):1647-1655.

ZHANG Y R, YOON N, HOLUSZKO M E., 2021. *Assessment of sortability using a dual-energy X-ray transmission system for studied sulphide ore. Minerals*. 11(5):490.

YEYU Y, WENBAO J, DAQIAN H, et al., 2021. *Feasibility study of a method for identification and classification of magnesium and aluminum with ME-XRT. Journal of Instrumentation*. 16(11), P11041.

DUVILLIER J, DIERICK M, DHAENE J, et al., 2018. *Inline multi-material identification via dual energy radiographic measurements. NDT & E International*. 94:120-125.

BAUER A, MAIER G, REITH-BRAUN M, et al., 2022. *Towards a feed material adaptive optical beltsorter: A simulation study utilizing a DEM-CFD approach. Powder Technology*. 411:117917.

PIEPER C, PFAFF F, MAIER G, et al., 2018. *Numerical modelling of an optical belt sorter using a DEM–CFD approach coupled with particle tracking and comparison with experiments.Powder Technology*. 340:181-193.

Küppers B, Schlögl S, Friedrich K, et al., 2021. *Influence of material alterations and machineimpairment on throughput related sensor-based sorting performance. Waste management& research.* 39(1):122-129.

ZHU DAO-YAO, LIANG DIAN-YIN, SHI PEI-wEI et al., 2016. *A study of the effect of ore jet nozzle structures on the jet flow field. Mining and Metallurgy.* 25(6):65-69.

CHEN Z, HE L, YE Y, et al., 2020. *Automatic sorting of fresh tea leaves using vision-based recognition method. Journal of Food Process Engineering*. 43(9), e13474.

ChEN Z, NI H, PEI X, et al., 2023. *Design and Fluid-Dynamic Analysis of a Flushing Nozzle for Drilling Applications. FDMP-Fluid Dynamics & Materials Processing*. 19:2953-2963.

ZHONG X, ZHU B, LIU M, et al., 2023. *Effect of nozzle inclination angle on characteristics of a gas jet in a gas-solid fluidized bed. Powder Technology*. 426:118572.

CRISTOFARO M, EDELBAUER W, KOUKOUVINIS P, et al., 2020. *A numerical study on the effect of cavitation erosion in a diesel injector. Applied Mathematical Modelling*. 78:200-216.

ZUCKER R D, BIBLARZ O., 2019. *Fundamentals of gas dynamics. John Wiley & Sons*.

CONSTANTIN P, FOIAS C., 1988. *Navier-stokes equations. University of Chicago press*.

AHMED O A B M, OVINIS M., 2019. *Evaluation of k-epsilon model for turbulent buoyant jet. Platform: A Journal of Engineering*. 3(2):55-64.

KANNAN B T, KARTHIKEYAN S, SUNDARARAJ S., 2017. *Comparison of turbulence models in simulating axisymmetric jet flow. In: Innovative Design and Development Practices in Aerospace and Automotive Engineering: I-DAD, February 22-24, 2016. Springer Singapore*. 401-407.

FLUENT A., 2023. *Ansys fluent theory guide. Ansys Inc*.

HATANAKA K, SAITO T., 2012. *Influence of nozzle geometry on underexpanded axisymmetric free jet characteristics. Shock Waves*. 22:427-434.

LAI G., 2023. *Sonic-supersonic jet flows from a two-dimensional nozzle. Journal of Differential Equations*. 360:287-313.

GEORGE J, NAIR P P, SOMAN S, et al., 2021. *Visualization of flow through planar double divergent nozzles by computational method. Journal of Visualization*. 24, 711-732.

DOI: 10.37190/ppmp/191375